Correspondence

Postarthroplasty Examination Using X-Ray Images

Kush R. Varshney*, *Student Member, IEEE*,
Nikos Paragios, *Senior Member, IEEE*, Jean-François Deux,
Alain Kulski, Rémy Raymond, Phillipe Hernigou, and
Alain Rahmouni

Abstract—**Arthroplasty, the implantation of prostheses into joints, is a surgical procedure that is affecting a larger and larger number of patients over time. As a result, it is increasingly important to develop imaging techniques to noninvasively examine joints with prostheses after surgery, both statically and dynamically in 3-D. The static problem is considered here, with the aim to create a 3-D shape model of the bone as well as the prosthesis using a set of 2-D X-rays from various viewpoints. The most important challenge to be addressed is the lack of texture, the most common feature to recover shape from multiple views. In order to overcome this limitation, we reformulate the problem using a novel multiview segmentation approach where an active contours 3-D surface evolution with level-set implementation is used to recover the shape of bones and prostheses in postoperative joints. The recovered shape may then be used to track 3-D motions in dynamic X-ray sequences to obtain kinematic information.**

Index Terms—**Active contours, multiview stereo reconstruction, orthopedics, X-ray imaging, three-dimensional (3-D) level-set methods.**

Fig. 1. X-ray images from rotating sensor of knee with prosthesis.

I. INTRODUCTION

Improvements in sanitation, nutrition, and treatment of infectious disease have resulted in a significant increase in life expectancy. However, with an aging population comes degenerative disease such as osteoarthritis, the deterioration of joints such as the knees and hips. In treating osteoarthritis, the final resort is arthroplasty, the implantation of artificial prostheses. Since 1994–1995, the number of hip and knee replacements has had a ten year increase of 94% in Australia, 87% in Canada, and similar increases in other countries such as New Zealand, Sweden, and the United States of America [1], [2]. In these countries, the crude rate for knee replacement is around 100 per 100 000 individuals [2].

*K. R. Varshney is with the Laboratory for Information and Decision Systems, Massachusetts Institute of Technology, Cambridge, MA 02139 USA (e-mail: krv@mit.edu).

N. Paragios is with the Laboratoire de Mathématiques Appliquées aux Systèmes, École Centrale Paris, 92290 Châtenay-Malabry Cedex, France and also with the GALEN Team, INRIA, 91893 Orsay Cedex, France (e-mail: nikos.paragios@ecp.fr).

J.-F. Deux is with the Assistance Publique-Hôpitaux de Paris, Centre Hospitalo-Universitaire Henri Mondor, Service d'Imagerie Médicale, 94010 Créteil Cedex, France, and also with UMR 7054, Centre National de la Recherche Scientifique, 94010 Créteil Cedex, France (e-mail: jean-francois.deux@hmn.aphp.fr).

A. Kulski, R. Raymond, A. Rahmouni, and P. Hernigou are with the Assistance Publique-Hôpitaux de Paris, Centre Hospitalo-Universitaire Henri Mondor, Service d'Imagerie Médicale, 94010 Créteil Cedex, France (e-mail: alain.kulski@hmn.aphp.fr; remy.raymond@hmn.aphp.fr; alain.rahmouni@hmn.aphp.fr; phillipe.hernigou@hmn.aphp.fr).

Color versions of one or more of the figures in this paper are available online at http://ieeexplore.ieee.org.

Digital Object Identifier 10.1109/TMI.2008.927341

Medical imaging plays two roles in arthroplasty. The first is in performing the surgery, where image guidance and automation are becoming routine [3]. The second is examination after surgery. During the life of the prosthesis, it is of clinical interest to characterize kinematics and prosthetic positioning through noninvasive examination of the joint [4]. We address the second, postsurgical application in this correspondence, as it continues to become more important.

X-ray imaging is the modality of choice when examining bones and the skeletal structure *in situ*. With the ultimate task being to understand the forces at work in the joint, we would like to determine the 3-D placement and movement of both the bones and prosthesis. This may be decomposed into a static phase of determining 3-D shape and a dynamic phase of tracking under the assumption of rigid body or nearly rigid body motion.

For the static phase, one possibility would be X-ray computed tomography (CT), if not for the high radiation dosage and cost incurred, and the streaking artifacts that arise in the presence of foreign metal objects when reconstructing CT volumes using conventional image formation techniques [5]. Thus, for the static phase, we turn to reconstruction from 2-D X-ray images acquired using a rotating sensor [6], [7]. A few images from such a dataset are shown in Fig. 1 for a knee joint with prosthesis made up of a tibial plate with stem and a curved femoral component. Such an approach involves a small amount of radiation as well as reasonable cost if the number of views is optimized.

For the dynamic phase, available data include movie sequences of 2-D X-ray images from a single viewpoint taken while the joint is used; some frames from a sequence of the knee are shown in Fig. 2. Using the 3-D shape recovered from the static phase, the remaining problem is 2-D/3-D registration and tracking, which has been addressed in the literature, e.g., [4], [8]–[10].

The task consists of recovering an articulated deformation of the prosthesis model such that in the image, the projection of the 3-D model

Fig. 2. Movie sequence of flexing knee joint.

coincides with or corresponds to prosthesis-like intensity regions. The model is to be deformed according to a parametric affine transformation. The definition of the cost function can be done either through boundary-based techniques (minimize the image gradient along the projection of the surface silhouette), segmentation-driven approaches (the interior silhouette region should consist of prosthesis-like image features), or an analysis by synthesis approach (given the viewpoint and the relative position of the sensor, generate a view and try to minimize the error between the image and the observation).

Furthermore, we can relate the two prosthesis components of the 3-D model assuming a fixed joint angle, and look for a constrained articulation-like rotation which will provide an image projection that is prosthesis-like in terms of visual characteristics for both components. This is a common problem in computer vision (articulated tracking), tractable in our case given that the estimation of parametric deformations is an over-constrained problem.

Our focus in this correspondence is on the static phase. 3-D shape reconstruction of bones from CT volumes is well-studied, but the problem using a small number of 2-D X-ray images from different viewpoints has not received as much attention. The problem of 3-D shape estimation from a set of 2-D images has received attention in the computer vision community in the context of optical imaging for objects such as statuettes and is given the name multiview stereo reconstruction, see [11] and references therein. However, assumptions relating to radiance, occlusion, etc. are included that do not necessarily apply when dealing with X-ray imaging. The problem using X-ray images in nondestructive testing for industrial object quality control is considered in [12].

For 3-D bone reconstruction from a few 2-D X-rays, methods exist that rely on fairly accurate prior shape models or atlases, e.g., [13]–[15] and references therein. Methods such as [16], [17] need no prior information, but perform 2-D segmentation on individual images separately and then interpolate to form a 3-D surface. In [18], the same approach is applied to determine the 3-D shape of the cement used to attach prostheses to bone. In this work, first reported in [19], we develop an active contours formulation for the 3-D shape recovery of bones and prostheses. We take the specifics of the application and imaging modality into account, do not rely on a prior 3-D shape model, and segment in 3-D from the outset rather than stitching together 2-D segmentations.

II. MULTIVIEW STEREO FROM X-RAYS

To recover the 3-D shape of bones and prostheses from X-rays, existing multiview stereo reconstruction methods cannot just be taken off the shelf. In this section, specific features present in X-ray imaging are discussed, followed by the proposal of a method matched to the modality.

A. X-Ray Modality

Many characteristics differentiate X-ray imaging from optical imaging (upon which multiview stereo reconstruction techniques are

based). If one bone is in front of another bone, there would be occlusion in an optical image, but the X-ray modality shows both bones with pixel intensities darkened in the overlap region. The effect is neither transparency nor shadowing, but can be interpreted as something similar. Another related feature is that the boundaries of the bones are darker than the centers. This does not change image to image, so a point on the surface of a bone may appear dark in one image and light in an image from a different viewpoint. Multiview stereo techniques based on local correspondence rely on the assumption that a point on the surface appears the same in all of the images in which it is visible and that radiance is locally computable [20], [21], thus not being applicable to 3-D reconstruction of bone from X-rays.

Prostheses appear dark and exhibit no texture; consequently, local correspondence is ill-posed for reconstructing the shape of prostheses. Prostheses are homogeneous in image intensity, but bones are not. The background is full of clutter and image intensities inside and outside the bone may be very similar. Inhomogeneity in bones, background clutter, and lack of occlusion are barriers to the direct application of region-based variational methods such as [22] to X-ray imaging.

"Shape from silhouette," a method for multiview stereo reconstruction that takes the intersection of cylinders or cones projected back from silhouettes of the object in each image as its shape estimate, is well matched to prostheses and can be applied readily, but it does not take prior information into account [23]. Edges stand out in X-ray images and have not been exploited much in previous work on multiview reconstruction. The edges of bones and prostheses, however, are not the only edges in X-rays; overlapping soft tissue also induces strong edges. Nevertheless, the use of edge features is an avenue that we pursue for this challenging application, combined with some region-based features and an approach inspired by shape from silhouette.

B. Multiview Geodesic Active Regions

An approach for 3-D shape reconstruction motivated specifically by the appearance of bones and prostheses in X-rays is now presented. Our variational method extends the 2-D geodesic active regions (GAR) functional to three dimensions by projecting cylinders or cones in a manner similar to shape from silhouette. Optimization is by surface evolution implemented using 3-D level sets. We focus on the knee joint, but the same methods may be applied to other joints that have had arthroplasty.

A set of 2-D images $\{I_1, I_2, \ldots, I_N\}$ with corresponding 2-D domains $\Omega_1, \Omega_2, \ldots, \Omega_N$ is given in the problem as input. Each Ω_i has local image coordinates (u_i, v_i). The goal is to determine the 3-D solid enclosed by a surface S that is depicted in the set of images. The surface S is in $\mathbb{R}^3$ with global Cartesian coordinates (x, y, z), or alternatively global cylindrical coordinates (r, θ, z). Within a 2-D plane Ω_i, a curve C_i is parameterized by a variable $s_i \in [0, 1]$ and has a line element ds_i.

The relationship between the global coordinates (x, y, z) and the local image coordinates (u_i, v_i) is assumed known or known approximately, i.e., the views or cameras are calibrated. These relationships are given by projections $\pi_i : \mathbb{R}^3 \rightarrow \Omega_i$. The mappings are not invertible in general because many different points in $\mathbb{R}^3$ project onto the same point in Ω_i. If the images are acquired using a rotating sensor with viewpoints in a ring outside the leg as in Fig. 1, then each Ω_i plane is parallel to the global z-axis and forms an angle θ_i to the x-z plane. In perspective projection, π_i is such that $u_i = (x \cos \theta_i + y \sin \theta_i)/w_i$ and $v_i = z/w_i$, where w_i is the relative perpendicular depth from the image plane Ω_i. In parallel projection, $u_i = x \cos \theta_i + y \sin \theta_i$ and $v_i = z$.

Before extending GAR to 3-D, the variational formulation is first reviewed in 2-D as the problem of image segmentation into two regions R and R^c. The GAR functional is the convex combination of two terms,

the geodesic active contours (GAC) functional and a region-based functional: $E_{\mathrm{GAR}}(C) = \alpha E_{\mathrm{GAC}}(C) + (1 - \alpha) E_{\mathrm{R}}(C)$ [24]. The GAC functional has minima where the curve C falls along strong edges [25]

$$E_{\mathrm{GAC}}(C) = \oint_C g(C(s))\, ds, \quad g(I) = \frac{1}{1 + |\nabla I|^p}$$

with $p \in [1, 2]$. To prevent local minima and fractally solutions, oftentimes a curve length penalty is also included:

$$E_{\mathrm{GAC}}(C) = \oint_C g(C(s))\, ds + c \oint_C ds.$$

The region-based portion assumes some prior knowledge regarding the image intensities of R and R^c. It is assumed that pixel values are independent given the region label and have probability distribution function $p_R(I(u, v))$ or $p_{R^c}(I(u, v))$. The functional, a log-likelihood ratio, is

$$E_{\mathrm{R}}(C) = -\iint\limits_R \log(p_R(I(u, v)))\, du\, dv$$
$$-\iint\limits_{R^c} \log(p_{R^c}(I(u, v)))\, du\, dv.$$

Starting from an initial curve, a curve evolution approach is taken to flow towards a minimum of the functional. Using a level-set implementation with the signed distance function $\varphi(u, v; t)$, the level-set update equation is $\varphi_t = F|\nabla\varphi|$, with

$$F(u, v)$$
$$= \alpha \left(\kappa \left(g(I(u, v)) + c \right) - \left\langle \nabla g(I(u, v)), \frac{\nabla \varphi(u, v)}{|\nabla \varphi(u, v)|} \right\rangle \right)$$
$$+ (1 - \alpha) \left(-\log(p_R(I(u, v))) + \log(p_{R_c}(I(u, v))) \right)$$

where κ is the curvature of C, and $\langle \cdot, \cdot \rangle$ indicates the inner product.

Reverting to the multiview problem, we would like to have one surface in 3-D and evolve that surface based on information provided by all of the images. All points on a line in 3-D map to a point (u_i, v_i) in Ω_i; our approach is to apply the GAR flow at (u_i, v_i) to all points (x, y, z) that project to it. The overall force applied to a point (x, y, z) is the superposition of forces from all N images.

We construct a multiview geodesic active regions functional with a GAC term and a region-based term. The GAC portion of the functional is

$$E_{\mathrm{GAC-MV}}(S) = \sum_{i=1}^{N} \oint_{C_i} g(C_i(s_i))\, ds_i + c \oint_{C_i} ds_i.$$

Making the assumption that the shape S has a pixel intensity distribution p_R when seen in an image, and the background has a distribution p_{R^c}, the region-based portion is

$$E_{\mathrm{R-MV}}(S) = -\sum_{i=1}^{N} \int\limits_{\pi_i(S)} \int \log(p_R(I_i(u_i, v_i)))\, du_i\, dv_i$$
$$-\sum_{i=1}^{N} \int\limits_{\Omega_i - \pi_i(S)} \int \log(p_{R^c}(I_i(u_i, v_i)))\, du_i\, dv_i.$$

Using a 3-D signed distance function $\varphi(x, y, z; t)$ the 3-D level-set update equation takes the form $\varphi_t = F|\nabla\varphi|$, with

$$F(x, y, z) = \alpha \sum_{i=1}^{N} \kappa \left(\left(g(I_i(u_i, v_i)) + c \right) \right.$$

$$\left. - \left\langle \nabla_i g(I_i(u_i, v_i)), \frac{\nabla_i \varphi(x, y, z)}{|\nabla_i \varphi(x, y, z)|} \right\rangle \right)$$
$$+ (1 - \alpha) \sum_{i=1}^{N} \left(-\log(p_R(I_i(u_i, v_i))) \right.$$
$$\left. + \log(p_{R_c}(I_i(u_i, v_i))) \right).$$

By ∇_i, we mean a gradient with respect to the u_i and v_i axes of Ω_i. The force has effect only in the direction normal to S in 3-D. Explicitly, $\partial\varphi(x, y, z)/\partial u_i = (\partial\varphi(x, y, z)/\partial x)\cos\theta_i + (\partial\varphi(x, y, z)/\partial y)\sin\theta_i$, and $\partial\varphi(x, y, z)/\partial v_i = \partial\varphi(x, y, z)/\partial z$.

The surface evolution couples information provided by each image; individual 2-D functionals for each image extend back in a cone or cylinder of influence in 3-D. It is in this way that the approach relates to shape from silhouette. Occlusions are not modeled for the reasons discussed in Section II-A.

III. PRELIMINARY RESULTS

This section shows preliminary results of multiview stereo reconstruction of prostheses and bones using the multiview GAR approach. Our data are X-ray image sets with different numbers of images covering the same total angle; the images are as in Fig. 1. As the sensor is sufficiently far from the knee joint, we use parallel projection, a valid assumption in X-ray images [26].
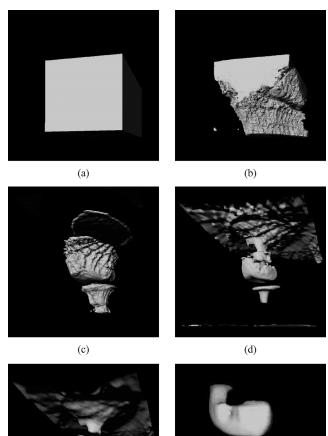
A. Prosthesis Reconstruction

First, the problem of recovering the 3-D shape of the femoral component and tibial plate of the knee prosthesis is addressed, treating soft tissue, bone, and air as background. No special initialization is required; a cube that projects to cover about half of an image is used. Although not completely accurate, in specifying the probabilities p_R and p_{R^c}, we take the pixels to be i.i.d. Gaussian with means μ_R for the prosthesis and μ_{R^c} for the background with common variance. The parameters for the Gaussian, same for all N region terms, are set prior to running the surface evolution based on pixel intensity values for prosthesis and nonprosthesis in the X-ray image dataset.

Several iterations of the surface evolution are shown in Fig. 3 for $N = 16$, starting from the initial cube. (The figure shows triangulated surfaces obtained from the implicit level-set representation by the marching cubes method.) A very small piece of the femur along with part of the black boundary is apparent in Fig. 3, but these pieces are disjoint from the prosthesis and easily discarded in Fig. 3(f). In the final 3-D reconstruction, the two pieces of the prosthesis have been recovered.

In order to evaluate the segmentations, a comparison is made to a manual segmentation of the prostheses from a CT volume of the same patient acquired on a different day. The knee is bent differently in the 2-D X-ray dataset and the CT volume dataset, so the two components of the prosthesis are examined separately. First a rigid registration is performed between the multiview GAR segmentation solution and the CT segmentation, and then symmetric volume difference is calculated. As seen in Fig. 4, the two are of the same general shape, confirming the validity of the solution.

Table I gives the symmetric volume difference results for different values of N. Some of the error is due to the hollowness of the stem of the tibial component and concavities in the femoral component that are not visible in the 2-D images used. With more images, the general trend is for performance to improve. The benefit of an increase in the number of views is more significant when the shape to be recovered is not rotationally symmetric. Performance on the tibial plate, the simpler and more rotationally symmetric shape, improves from $N = 2$ to $N = 8$
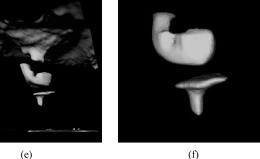
Fig. 3. For $N = 16$, (a)–(e) iterations of surface evolution in raster scan order and (f) reconstructed shape of the prosthesis.
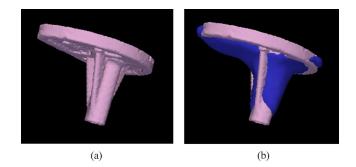

Fig. 4. Comparison of (a) tibial plate segmentation from CT data and (b) $N = 16$ solution overlaid.

but then saturates. Performance on the more complicated femoral component continues to improve from $N = 4$ to $N = 20$. The decrease in performance from $N = 2$ to $N = 4$ is not significant as both solutions are poor.

One way to look at the model selection problem of choosing N is through criteria such as the Akaike information criterion (AIC) [27], which trade the complexity of a model and its goodness of fit. The AIC can be approximated by the sum of the symmetric volume difference

TABLE I
SYMMETRIC VOLUME DIFFERENCE FOR DIFFERENT VALUES OF N

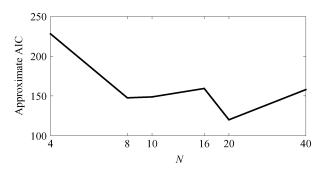| N	Δ_θ (rad)	Symmetric Vol. Diff. (cm^3)		
		Femoral	Tibial	Total
2	1.52	162.7	49.0	211.7
4	0.76	185.0	35.2	220.2
8	0.38	100.4	31.2	131.6
10	0.304	100.3	28.5	128.8
16	0.19	97.4	30.0	127.4
20	0.152	50.5	29.5	80.0
40	0.076	51.5	26.5	78.0

Fig. 5. Approximate Akaike information criterion as a function of the number of views N.

and $2N$, assuming errors are independent and distributed according to a generalized Gaussian distribution with small shape parameter. Approximate AIC values are plotted in Fig. 5; $N = 20$ has the smallest AIC. For our application, the criterion is more complicated because certain errors are worse than others and the cost and radiation dosage associated with N must also be taken into account; the quantification of these factors is a nontrivial task.

B. Bone Reconstruction

The pixel intensity in X-ray images of bones is not homogeneous throughout the bone, but follows a predictable pattern. The boundary is dark and the shading gets lighter as the distance away from the boundary increases. In other words, pixel intensity values generally increase as a function of signed distance.

When reconstructing the 3-D shape of bones, we set p_R to account for this phenomenon. We once again take p_R to be Gaussian and independent among different pixels, but not identically distributed. We put in a spatially varying mean $\mu_R(\varphi_i)$ that is a function of signed distance.

The signed distance function $\varphi(x, y, z)$ of the surface evolution is in 3-D, but we need distances in the Ω_i domains. Thus, the 3-D signed distance is projected down to the plane Ω_i as $\varphi_i(x, y, z)$ for each i. In this work, $\mu_R(\varphi_i)$ is a simple parameterized function of the form $\mu_R(\varphi_i) = \eta_1 - \eta_2 e^{-(\varphi_i + \eta_3)^2}$ with parameters set to fit pixel intensity values in one manually-segmented 2-D X-ray.

We obtain 3-D shapes such as those in Fig. 6, treating the bone and prosthesis as the object of interest and everything else as background. Fig. 6(a) shows the tibia and fibula, whereas Fig. 6(b) shows the femur. The circular fields of view in the images leave an artifact along the boundary as part of the surface. The tibia and fibula cannot be distinguished in X-rays from certain angles. Consequently, they are not completely separated in Fig. 6(a).

The recovered shapes are qualitatively similar to the shapes seen in the CT data. The solutions for bones are quantitatively worse than the solutions for prostheses alone, which were given in Section III-A. It is difficult to give precise numerical symmetric volume difference results
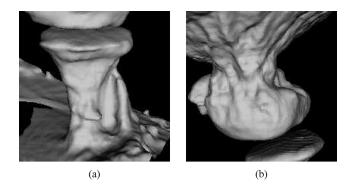
Fig. 6. Reconstructed shape for $N = 16$ of the (a) tibia and fibula, and (b) femur.

here due to the boundary artifacts in the solutions. The general trend here is also improved performance with increased N.

The main sources of error in bone reconstruction are interference from soft tissue and the lack of consistency in bone appearance from image to image. Obtaining the shape of the bones is more difficult than obtaining the shape of the prostheses. Qualitative and quantitative comparisons between solution shapes and the CT volume suggest that there is reason to be optimistic about the proposed approach but that there is also much room for improvement.

IV. CONCLUSION

Our main objective in this correspondence has been to inform the medical imaging community of an emerging and clinically important problem. Even with a fairly simplistic active contours formulation, we have obtained promising preliminary results. However, the comparison to CT segmentation indicates that there is much room for improvement. Reconstructing the 3-D shape of prostheses and even more so of bones from multiple X-ray images is not straightforward. This is caused by four factors: radiance is not locally computable; prostheses are textureless; bones are inhomogeneous; and the background is cluttered. In spite of these factors, however, we feel that better results can be obtained. Improvements may be made by including separate partitions for three classes: prosthesis, bone, and background, via multiphase segmentation, i.e., segmentation with more than two categories. Enhancements may also be made by improving pixel intensity models p_R and p_{R^c} via learning from data [28] or using generative models based on X-ray absorption, by including shape priors in the context of level-set representations [28], [29], or along with more efficient optimization techniques from discrete optimization [30]. Instead of using the 2-D GAR functional as a foundation for the 3-D problem, an approach that jointly optimizes pixel intensity could also be used [31]. The development of a full system including both static and dynamic phases integrated with the inference of velocities, accelerations, and forces is certainly within grasp.

REFERENCES

[1] Australian Orthopaedic Association National Joint Replacement Registry Australian Orthopaedic Assoc., Adelaide, Australia, Annu. Rep., 2006.

[2] Canadian Joint Replacement Registry Canadian Institute for Health Information, Toronto, ON, Canada, Annu. Rep. Hip Knee Replacements, 2006.

[3] F. Rodriguez y Baena, "Man and the machine," *IET Comput. Contr. Eng.*, pp. 28–31, Oct./Nov. 2006.

[4] S. Zuffi, A. Leardini, F. Catani, S. Fantozzi, and A. Cappello, "A model-based method for the reconstruction of total knee replacement kinematics," *IEEE Trans. Med. Imag.*, vol. 18, no. 10, pp. 981–991, Oct. 1999.

[5] R. J. Murphy, S. Yan, J. A. O'Sullivan, D. L. Snyder, B. R. Whiting, D. G. Politte, G. Lasio, and J. F. Williamson, "Pose estimation of known objects during transmission tomographic image reconstruction," *IEEE Trans. Med. Imag.*, vol. 25, no. 10, pp. 1392–1404, Oct. 2006.

[6] M. Zellerhoff, B. Scholz, E.-P. Rührnschopf, and T. Brunner, "Low contrast 3D-reconstruction from C-arm data," *Proc. SPIE*, vol. 5745, pp. 646–655, 2005.

[7] H. Kroon, N. Schoumans, and R. Snoeren, "Image quality simulation and verification of X-ray volume imaging systems," *Proc. SPIE*, vol. 6142, p. 614250, 2006.

[8] Á. Czopf, C. Brack, M. Roth, and A. Schweikard, "3D-2D registration of curved objects," *Periodica Polytechnica Elec. Eng.*, vol. 43, no. 1, pp. 19–41, 1999.

[9] J. Weese, T. M. Buzug, G. P. Penney, and P. Desmedt, "2D/3D registration and motion tracking for surgical interventions," *Philips J. Res.*, vol. 51, no. 2, pp. 299–316, 1998.

[10] D. Tomaževič, B. Likar, and F. Pernuš, "3-D/2-D registration by integrating 2-D information in 3-D," *IEEE Trans. Med. Imag.*, vol. 25, no. 1, pp. 17–27, Jan. 2006.

[11] S. M. Seitz, B. Curless, J. Diebel, D. Scharstein, and R. Szeliski, "A comparison and evaluation of multi-view stereo reconstruction algorithms," in *Proc. IEEE Comput. Soc. Conf. Comput. Vis. Pattern Recognit.*, New York, Jun. 2006, vol. 1, pp. 519–526.

[12] C. Lehr and C.-E. Liedtke, "3D reconstruction of volume defects from few X-ray images," in *Proceedings of the 8th International Conference on Computer Analysis of Images and Patterns*. New York: Springer, 1999, vol. 1689, Lecture Notes Comput. Sci., pp. 275–284.

[13] H. Lamecker, T. H. Wenckebach, and H.-C. Hege, "Atlas-based 3D-shape reconstruction from X-ray images," in *Proc. Int. Conf. Pattern Recognit.*, Aug. 2006, vol. 1, pp. 371–374.

[14] G. Zheng and L.-P. Nolte, "Surface reconstruction of bone from X-ray images and point distribution model incorporating a novel method for 2D-3D correspondence," in *Proc. IEEE Comp. Soc. Conf. Comput. Vis. Pattern Recognit.*, New York, Jun. 2006, vol. 2, pp. 2237–2244.

[15] X. Dong, M. A. Gonzalez Ballester, and G. Zheng, "Automatic extraction of femur contours from calibrated fluoroscopic images," in *Proc. IEEE Workshop Applicat. Comput. Vis.*, Austin, TX, Feb. 2007, p. 55.

[16] L. Caponetti and A. M. Fanelli, "Computer-aided simulation for bone surgery," *IEEE Comput. Graph. Appl.*, vol. 13, no. 6, pp. 86–92, Nov. 1993.

[17] B. Nikkhade-Dehkori, M. Bro-Nielsen, T. Darvann, C. Gramkow, N. Egund, and K. Hermann, "3D reconstruction of the femoral bone using two X-ray images from orthogonal views," *Proc. Comput. Assist. Radiol.*, pp. 26–29, 1996.

[18] M. de la Fuente, J. A. K. Ohnsorge, E. Schkommodau, S. Jetzki, D. C. Wirtz, and K. Radermacher, "Fluoroscopy-based 3-D reconstruction of femoral bone cement: A new approach for revision total hip replacement," *IEEE Trans. Biomed. Eng.*, vol. 52, no. 4, pp. 664–675, Apr. 2005.

[19] K. R. Varshney, N. Paragios, A. Kulski, R. Raymond, P. Hernigou, and A. Rahmouni, "Multi-view stereo reconstruction of total knee replacement from X-rays," in *Proc. IEEE Int. Symp. Biomed. Imag.*, Arlington, VA, Apr. 2007, pp. 1148–1151.

[20] K. N. Kutulakos and S. M. Seitz, "A theory of shape by space carving," *Int. J. Comput. Vision*, vol. 38, no. 3, pp. 199–218, 2000.

[21] O. Faugeras, J. Gomes, and R. Keriven, "Computational stereo: A variational method," in *Geometric Level Set Methods in Imaging, Vision, and Graphics*, S. Osher and N. Paragios, Eds. New York: Springer-Verlag, 2003, pp. 343–360.

[22] A. J. Yezzi, Jr. and S. Soatto, "Stereoscopic segmentation," *Int. J. Comput. Vis.*, vol. 53, no. 1, pp. 31–43, 2003.

[23] A. Laurentini, "The visual hull concept for silhouette-based image understanding," *IEEE Trans. Pattern Anal. Mach. Intell.*, vol. 16, no. 2, pp. 150–162, Feb. 1994.

[24] N. Paragios and R. Deriche, "Geodesic active regions: A new framework to deal with frame partition problems in computer vision," *J. Vis. Commun. Image Representation*, vol. 13, pp. 249–268, 2002.

[25] V. Caselles, R. Kimmel, and G. Sapiro, "Geodesic active contours," *Int. J. Comput. Vis.*, vol. 22, pp. 61–79, 1997.

[26] X. Hu and N. Ahuja, "Motion estimation under orthographic projection," *IEEE Trans. Robot. Automat.*, vol. 7, no. 6, pp. 848–853, Dec. 1991.

[27] H. Akaike, "A new look at the statistical model identification," *IEEE Trans. Automat. Control*, vol. AC-19, no. 6, pp. 716–723, Dec. 1974.

[28] M. E. Leventon, O. Faugeras, W. E. L. Grimson, and W. M. Wells, III, "Level set based segmentation with intensity and curvature priors," in *Proc. Workshop Math. Methods Biomed. Image Anal.*, Hilton Head, SC, Jun. 2000, pp. 4–11.

[29] M. Rousson and N. Paragios, "Prior knowledge, level set representations & visual grouping," *Int. J. Comput. Vis.*, vol. 76, no. 3, pp. 231–243, 2008.

[30] M. Sardarescu, N. Paragios, N. Komodakis, R. Raymond, P. Hernigou, and A. Rahmouni, "Knee reconstruction through efficient linear programming," in *Proc. IEEE Int. Symp. Biomed. Imag.*, Paris, France, May 2008, pp. 664–667.

[31] C. V. Alvino and A. J. Yezzi, Jr., "Tomographic reconstruction of piecewise smooth images," in *Proc. IEEE Comput. Soc. Conf. Comput. Vis. Pattern Recognit.*, Washington, DC, Jun.–Jul. 2004, vol. 1, pp. 576–581.